Journal of Zhejiang University-SCIENCE A (Applied Physics & Engineering)
ISSN 1673-565X (Print); ISSN 1862-1775 (Online)
www.jzus.zju.edu.cn; www.springerlink.com
E-mail: jzus@zju.edu.cn

A deep-learning method for evaluating shaft resistance of the cast-in-site pile on reclaimed ground using field data*

Sheng-liang LU[1,2,3], Ning ZHANG[†‡1,2], Shui-long SHEN[1,2,4], Annan ZHOU[4], Hu-zhong LI[5]

[1]*Department of Civil and Environmental Engineering, College of Engineering, Shantou University, Shantou 515063, China*

[2]*Key Laboratory of Intelligence Manufacturing Technology of Ministry of Education, Shantou University, Shantou 515063, China*

[3]*Department of Architecture and Civil Engineering, Wenzhou Vocational and Technical College, Wenzhou 325000, China*

[4]*Discipline of Civil and Infrastructure, School of Engineering, Royal Melbourne Institute of Technology (RMIT), Victoria 3001, Australia*

[5]*Wenzhou Huabang Engineering Project Management Co., Ltd., Wenzhou 325207, China*

[†]E-mail: zhangning@stu.edu.cn

Received Oct. 24, 2019; Revision accepted Mar. 20, 2020; Crosschecked May 27, 2020

Abstract: This study proposes a deep learning-based approach for shaft resistance evaluation of cast-in-site piles on reclaimed ground, independent of theoretical hypotheses and engineering experience. A series of field tests was first performed to investigate the characteristics of the shaft resistance of cast-in-site piles on reclaimed ground. Then, an intelligent approach based on the long short term memory deep-learning technique was proposed to calculate the shaft resistance of the cast-in-site pile. The proposed method allows accurate estimation of the shaft resistance of cast-in-site piles, not only under the ultimate load but also under the working load. Comparisons with empirical methods confirmed the effectiveness of the proposed method for the shaft resistance estimation of cast-in-site piles on reclaimed ground in offshore areas.

Key words: Deep-learning method; Cast-in-site pile; Shaft resistance; Field test; Reclaimed ground
https://doi.org/10.1631/jzus.A1900544 **CLC number:** TU473.1

1 Introduction

Reclaimed ground in offshore areas is usually characterised by a high water content, high compressibility, and poor mechanical properties (Ji et al., 2011; Formela et al., 2015; Nonaka et al., 2017; Shen et al., 2018). When reclaimed ground directly acts as the foundation subsoil, the infrastructure may be damaged, e.g. by cracking, overturning, and differential settlement (Shen et al., 2017; Lyu et al., 2020b, 2020c; Wu et al., 2020). Therefore, improvement of reclaimed ground is in high demand for infrastructure construction of cities in the offshore areas of China, such as Tianjin (Yan and Chu, 2005; Cai et al., 2018), Wenzhou (Wang XW et al., 2019; Zhang et al., 2019), and Shenzhen (Li et al., 2014; Wang ZF et al., 2019; Elbaz et al., 2020). Among the multiple ground improvement techniques, such as geotextiles (Zhang et al., 2015; Lyu et al., 2019a), prefabricated vertical drains (PVD) (Shen et al., 2005; Chai et al., 2018; Lyu et al., 2019b, 2020a), jet grouting (Wang et al., 2018), and the cast-in-site pile (Zhou M et al., 2016), the cast-in-site pile is one of the most popular techniques and features extensive reinforcement scope and an excellent improvement effect. In the case of soft ground, the pile usually relies on the shaft resistance from soils to provide support for buildings. However, the complex interactions between the pile and multi-layer soils make it difficult to accurately

‡ Corresponding author
* Project supported by the Research Funding of Shantou University for New Faculty Member (No. NTF19024-2019) and the National Nature Science Foundation of China (No. 41372283)
ORCID: Ning ZHANG, https://orcid.org/0000-0001-5302-600X

estimate the shaft resistance of piles. Typically, the determination of the shaft resistance of a cast-in-site pile is mainly dependent on an empirical formulation or field tests, which can result in uncertainty for the pile design or prolong the construction. Additionally, conventional methods for calculating the shaft resistance focus on normal or over-consolidated soils (Yao et al., 2008a, 2008b; Zhou JJ et al., 2013; Zhou AN et al., 2016, 2018; Yin et al., 2017, 2018a, 2018b; Jin et al., 2018a, 2018b; Kong et al., 2019). For reclaimed ground in an offshore area, under-consolidated soil is common because the ground was probably under the sea or water level (Liu et al., 2004; Li et al., 2005; Behrmann and Meissl, 2012; Sarir et al., 2019; Xu et al., 2019; Zhou et al., 2019). Therefore, the popular empirical formulation with experimental parameters usually fails to accurately provide the shaft resistance.

Popular empirical methods include the α (Randolph and Murphy, 1985), β (Ling et al., 2018), the Federal Highway Administration workbook (FHWA) (O'Neill and Reese, 1999), the Norwegian Geotechnical Institute (NGI) (Karlsrud et al., 2005), European (de Kuiter and Beringen, 1979), and French (Bustamante and Gianeselli, 1982) methods. Most of these methods can be used only for ultimate shaft-resistance estimation based on field test results and the limit equilibrium theory. Therefore, the conventional methods can only be used for roughly estimating the ultimate shaft resistance and are unsuitable for investigating the variation of the shaft resistance under the working load, which is significant for understanding the mechanism of shaft resistance. Moreover, the empirical methods depend greatly on various simplification rules, such as the simplified strata and force equilibrium, reducing the accuracy and confidence levels of calculated results. Alternatively, machine learning techniques are effective for determining the shaft resistance because of their strong nonlinear mapping ability. The application of neural networks for estimating the bearing capability of piles started in the 1990s (Chan et al., 1995; Goh, 1996; Lee and Lee, 1996; Teh et al., 1997; Abu Kiefa, 1998; Atangana Njock et al., 2020) and was recently revived as neural networks have evolved. Owing to their strong capability of nonlinear representation, neural networks can extract the hidden principles of the working shaft resistance, strata, and working load without simplification; thus, the results are more reliable than those of empirical methods. However, most research attention is still paid to the estimation of the ultimate shaft resistance or parameters via conventional methods with the aim of analysing the safety of different types of piles. Goh et al. (2005) combined the Bayesian method and a neural network to predict the parameter alpha via experimental methods. Ghorbani et al. (2018) used an adaptive neuro-fuzzy inference system to predict the ultimate bearing capability of multiple piles. Ardalan et al. (2009), Park and Cho (2010), Shahin (2010), Alkroosh and Nikraz (2012), and Baziar et al. (2012) also estimated the ultimate shaft resistance of piles. In these studies, the input data did not include the mechanical properties of the soils, such as the undrained shear strength, friction angle, and cohesion, although these are considered to significantly affect the shaft resistance in experimental and analytical methods. Furthermore, the existing neural network methods ignore the interaction among the strata owing to the nature of topological structures.

In the present study, a new method called the long short term memory (LSTM) deep-learning technique was employed to estimate the shaft resistance and axial force of cast-in-site piles. This is a popular method for sequenced artificial intelligence tasks, e.g. natural language processing (Gers et al., 2003) and speech recognition (Sak et al., 2014). In contrast to the existing intelligent method, the LSTM method considers the interaction among different strata using specified gate cells. Recently, the LSTM network has been employed in civil engineering for other problems, e.g. soil moisture estimation (Fang et al., 2019) and determination of the hydromechanical coupling effect of porous media (Wang and Sun, 2018). However, few investigations have been performed on the shaft resistance evaluation of cast-in-site piles using the LSTM deep-learning method.

The objective of this study was to evaluate the shaft resistance of cast-in-site piles on reclaimed ground via field tests, using the LSTM deep-learning method. In this method, the mechanical properties of the soils are used as the input data. First, field tests were designed and conducted to investigate the shaft resistance and axial force of cast-in-site piles under different loads on the reclaimed ground. Then, the empirical methods were used to estimate the ultimate

bearing capacity of the pile, and the results were compared with the measured data. Subsequently, an LSTM method was developed and employed to predict the shaft resistance and axial force of the pile, not only under the working load but also under the ultimate load.

2 Field experiments

2.1 Site details

The field site contained reclaimed ground located along the offshore area in Wenzhou City, Zhejiang Province, China. The strata comprised multi-layer soft soils with poor mechanical properties. From top to bottom, these soft soils were backfill, marine mucky clay, silty clay, clay, silty clay with gravel, and weathered quartzite, according to drill hole sampling. Fig. 1 depicts the local ground profile around the field site. The maximum thickness of the soft reclaimed ground was >70 m (referring to the depth below the ground), which is typical for extremely thick soft soil on reclaimed ground.

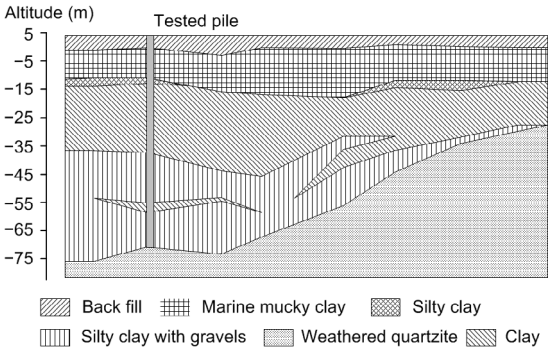

Fig. 1 Reclaimed ground profile around the field site

2.2 Soil properties

The soil properties were evaluated via laboratory tests, including triaxial and undrained consolidation test and routine analysis tests. The basic mechanical and physical properties of the soils are presented in Fig. 2. The marine mucky clay with a thickness of >10 m exhibited high compressibility, high water content, and the poorest mechanical properties. Generally, the soils at the field site were characterised by high compressibility and low mechanical indices. The relationship between the void ratio and the pressure is presented in Fig. 3. As shown, all the soils at the field site were in a state of under-consolidation. Compared with normally consolidated and over-consolidated soils, soils in the under-consolidated state exhibit a significantly different response to load.

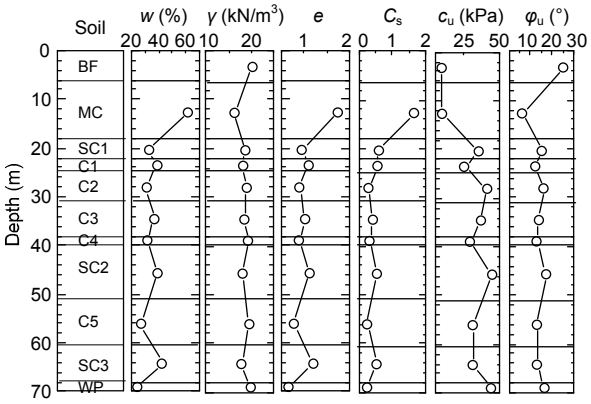

Fig. 2 Mechanical and physical properties of soils in the reclaimed ground

BF: back fill; MC: marine mucky clay; SC: silty clay; C: clay; WP: weathered quartzite; w: water content; γ: unit weight; e: void ratio; C_s: compressibility index; c_u: cohesion; φ_u: friction angle

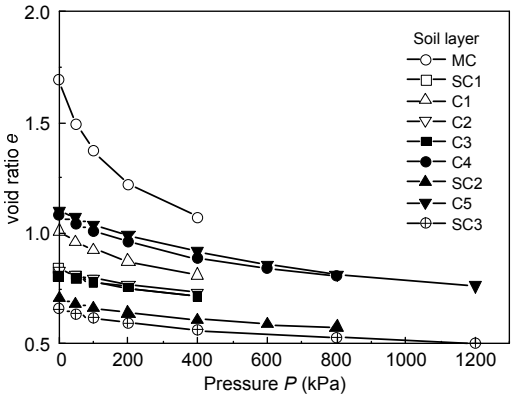

Fig. 3 Relationship between the void ratio and pressure for different soils

2.3 Experiment program

Eight piles labelled P16–P23 were arranged at intervals of 4 m, as shown in Fig. 4a. Considering similar geological conditions and cost control, only P16 was measured using stress gauges to evaluate the axial force of the pile at different depths. The stress gauges were intended to be installed at the soil interfaces. When the thickness of the soil exceeded 10 m, an additional stress gauge was installed in the middle

of the soil. A total of 13 stress gauges were employed, as shown in Fig. 4b. Fig. 4c presents the field situation of the finished cast-in-site pile P16.

Then, 28 d after all the piles were constructed, static loading tests were performed to investigate the changes in the shaft resistance and ultimate loading capacities of the cast-in-site piles on the reclaimed ground. Figs. 4d and 4e show the static loading test. The load of the concrete blocks was passed to the testing piles through a hydraulic jack. The loads were applied in a stepwise manner until the piles collapsed, with 800 kN at each step (approximately 10% of the pre-estimated ultimate loading capacity). The next load was applied after the measured increment of the displacement was <0.1 mm twice continuously within 2 h. The test was stopped when the displacement of the pile at the next load was twice the displacement at the former load and the pile exhibited continuous deformation for 24 h or when the total settlement surpassed 40 mm and kept increasing, in accordance with the Chinese code JGJ106-2014 (MOHURD, 2014). After the loading process, the piles were unloaded in one direct step. The unloading process was not considered, because the piles were loaded to collapse.

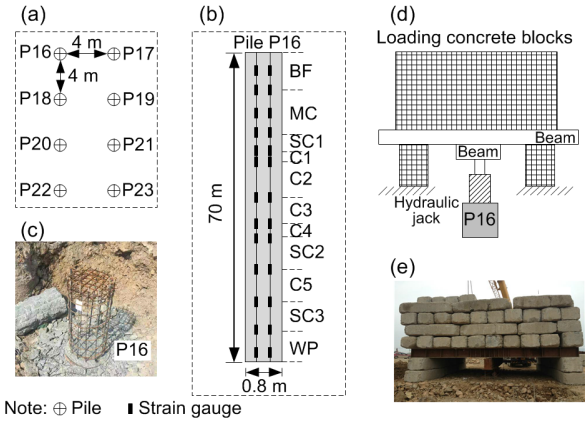

Fig. 4 Sketch of the field test program and site photographs: (a) layout of the tested piles; (b) size of pile P16 and installation of the stress gauges; (c) photograph of pile P16; (d) sketch map of the static loading tests; (e) photograph of the static loading tests

2.4 Experimental

2.4.1 Load–displacement response

Fig. 5 presents the curves for the loads and settlements of eight piles (P16–P23) in the static loading tests. The eight cast-in-site piles exhibited similar load–displacement responses under similar geological conditions and the same construction techniques. The settlements of all the cast-in-site piles exhibited an approximately linear increase when the load was <4500 kN, indicating that the shaft resistance of the piles was maintained and the piles supported the load. After the load exceeded 4500 kN, the deformation rates of all the piles increased, reaching a peak value of approximately 8000 kN. This suggests that the soils around the piles underwent plastic deformation and the pile tip resistances increased. Generally, the settlements of piles gradually increase with an increase in the static loads without any rapid variation. These are defined as the gradual-variation type in the Chinese code JGJ106-2014 (MOHURD, 2014). Therefore, the estimated ultimate load is determined when the total settlement of the piles surpasses 40 mm, according to the same Chinese code. The estimated ultimate load was 8000 kN in our case. Generally, the cast-in-site piles in the field tests provided sufficient support to the upper infrastructures, according to the load–displacement response.

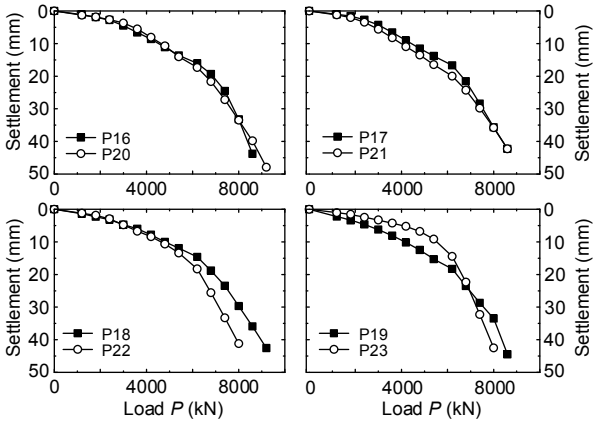

Fig. 5 Relationship between the load and settlement of the piles in the static loading tests

2.4.2 Axial force

During the static loading tests, the axial forces along pile P16 under different loads were simultaneously measured using the pre-installed stress gauges, as shown in Fig. 6. Under each load, the axial force decreased with an increase in the pile length, indicating that the shaft resistances of the different soils together supported the load. The slope of the axial force at the top of the pile was nearly identical under different loads in locations where backfill and

marine mucky clay were present. This indicates that the shaft resistance of the backfill and marine mucky clay was fully utilised at a load of 2000 kN. With an increase in the load, the shaft resistance of this part of the pile exhibited no changes. In contrast, the slopes of the axial force kept decreasing when the pile lengths were >20 m under different loads. The decreasing slope of the axial force indicated the increase in the shaft resistance of the soils for this part of the pile. Additionally, the axial force increased with the loads at the end of the pile, indicating that the tip resistance of the pile started to develop and share parts of the loads. The maximum tip resistance was only 900 kN, which was only 10% of the ultimate load. Therefore, the cast-in-site pile mainly relied on the shaft resistance to support the upper loads.

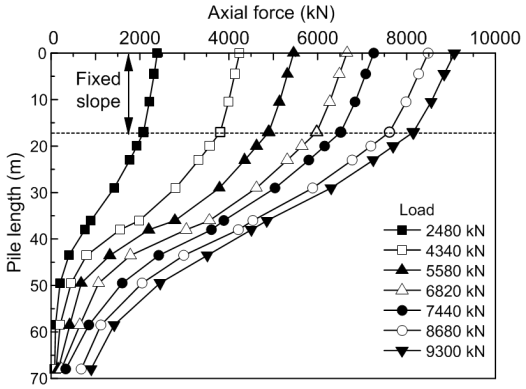

Fig. 6 Axial force development along pile P16 under different loads

2.4.3 Shaft resistance

The shaft resistance (τ_i) of the pile from the ith layer of soils was calculated using the axial force, as follows:

$$\tau_i = \frac{F_i - F_{i-1}}{h_i p}, \tag{1}$$

where F_i represents the axial force at the top of the ith layer of soil, h_i represents the thickness of the ith layer of soil, and p represents the circle perimeter of the pile.

Fig. 7 presents the shaft resistance of pile P16 under different loads. The trends of the shaft resistance versus the depth are in accordance with those of the axial force in Fig. 6. The shaft resistances changed little at the top of the pile but increased significantly in the middle part with the increasing loads. This phenomenon indicates that cast-in-site piles can support the upper loads at the field site containing reclaimed ground.

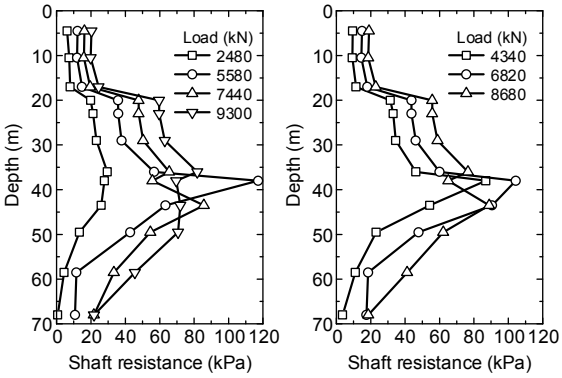

Fig. 7 Shaft resistances along pile P16 under different loads

3 Ultimate shaft resistance assessment

The ultimate shaft resistances were evaluated using empirical methods, including the α method (Randolph and Murphy, 1985) and the β method (Ling et al., 2018). The formulas for these two methods are as follows:

$$\begin{aligned} &\tau_{\max} = \alpha S_{\mathrm{u}} \quad (\alpha \text{ method}), \\ &\tau_{\max} = \beta \sigma'_{\mathrm{v}} = K_0 \tan\phi' \sigma'_{\mathrm{v}} \quad (\beta \text{ method}), \end{aligned} \tag{2}$$

where $\tau_{\max}$ represents the ultimate shear resistance at the interface between the soils and the pile, S_{u} represents the undrained shear strength of the soils, ϕ' represents the pile–soil interface friction angle, σ'_{v} represents the vertical effective stress, and α and β represent the strength coefficients. α is determined via the American Petroleum Institute (API) method (Randolph and Murphy, 1985) as follows:

$$\alpha = 0.5(S_{\mathrm{u}} / \sigma'_{\mathrm{v}})^{-0.5}. \tag{3}$$

K_0 is the coefficient of earth pressure at rest, which is estimated as follows (Mayne and Kulhawy, 1982):

$$K_0 = (1 - \sin\varphi)\mathrm{OCR}^{\sin\varphi}, \tag{4}$$

where OCR represents the over-consolidation ratio, and φ represents the effective friction angle. ϕ' can be taken equal to φ. The undrained shear strength of the soil (S_u) is calculated as follows (Ma et al., 2014):

$$S_u = c_u + \sigma_3 \tan\varphi_u, \tag{5}$$

where c_u represents the cohesion under undrained conditions, φ_u represents the friction angle, and σ_3 represents the minimum principle stress of the soil, which is estimated as

$$\sigma_3 = \frac{1+2K_0}{3}\sigma'_v. \tag{6}$$

The estimated undrained shear strengths of the soils are presented in Fig. 8. The strength generally increased with the depth, although the strength of the marine mucky clay was relatively low at a depth of 20 m.

The shaft resistances of pile P16, which were separately calculated using the α method and the β method, are presented in Fig. 9. Generally, empirical methods are effective for evaluating the shaft resistance of a pile when the depth is <50 m. However, biases arose for both empirical methods when the depth was <20 m and >50 m. These biases are attributed to the complex geological conditions on the reclaimed ground, which made the empirical methods with the ideal hypothesis unsuitable.

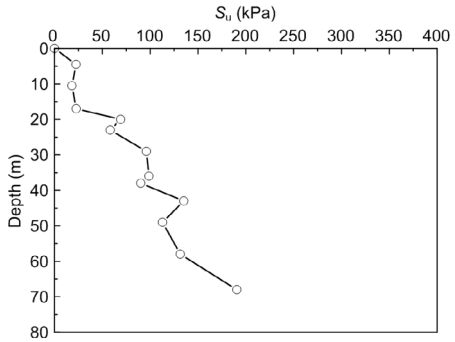

Fig. 8 Undrained shear strengths of soils at different depths at the field site

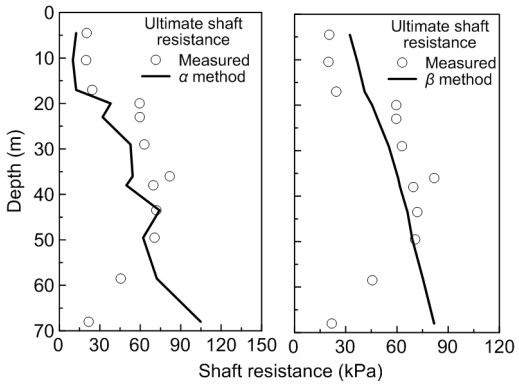

Fig. 9 Shaft resistances under different loads for pile P16 evaluated using different methods

4 Intelligent approach: LSTM modelling

4.1 Methodology

In the LSTM deep-learning method, the key for learning sequenced behaviours is a special unit called the LSTM unit. The LSTM units are interconnected along the time dimension to reflect the effect of the historical data on the current or future data. Fig. 10 shows the two-layered topological structure of the LSTM network.

The typical LSTM unit is composed of an input gate, an output gate, a forget gate, and a unit input. Let us suppose $\boldsymbol{X}^t$ as the input data and $\boldsymbol{y}_L{}^t$ as the output data for a simplified LSTM unit at time t. After the input data $\boldsymbol{X}^t$ and historical data $\boldsymbol{y}^{t-1}$ are imported into LSTM units, the following calculations are performed.

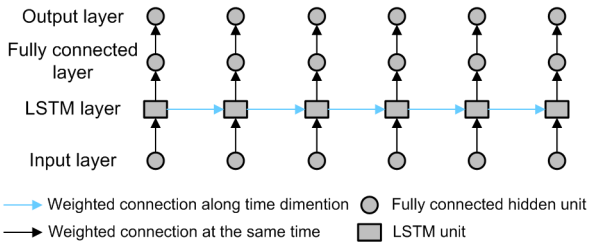

Fig. 10 Two-layered topological structure of the LSTM network

$$\begin{aligned}
&\overline{\boldsymbol{i}^t} = \boldsymbol{W}_i \times \boldsymbol{X}^t + \boldsymbol{R}_i \times \boldsymbol{y}_L{}^{t-1} + \boldsymbol{b}_i \quad \Rightarrow \boldsymbol{i}^t = S(\overline{\boldsymbol{i}^t}),\\
&\overline{\boldsymbol{f}^t} = \boldsymbol{W}_f \times \boldsymbol{X}^t + \boldsymbol{R}_f \times \boldsymbol{y}_L{}^{t-1} + \boldsymbol{b}_f \Rightarrow \boldsymbol{f}^t = S(\overline{\boldsymbol{f}^t}),\\
&\overline{\boldsymbol{o}^t} = \boldsymbol{W}_o \times \boldsymbol{X}^t + \boldsymbol{R}_o \times \boldsymbol{y}_L{}^{t-1} + \boldsymbol{b}_o \quad \Rightarrow \boldsymbol{o}^t = S(\overline{\boldsymbol{o}^t}),\\
&\overline{\boldsymbol{z}^t} = \boldsymbol{W}_z \times \boldsymbol{X}^t + \boldsymbol{R}_z \times \boldsymbol{y}_L{}^{t-1} + \boldsymbol{b}_z \quad \Rightarrow \boldsymbol{z}^t = T(\overline{\boldsymbol{z}^t}),\\
&\boldsymbol{c}^t = \boldsymbol{i}^t \odot \boldsymbol{z}^t + \boldsymbol{c}^{t-1} \odot \boldsymbol{f}^t,\\
&\boldsymbol{y}_L{}^t = T(\boldsymbol{c}^t) \odot \boldsymbol{o}^t.
\end{aligned} \tag{7}$$

Here, $\boldsymbol{W}_i$, $\boldsymbol{W}_o$, $\boldsymbol{W}_f$, and $\boldsymbol{W}_z$ represent the weights of the input data for the input gate, output gate, forget gate,

and input unit, respectively. $\boldsymbol{R}_i$, $\boldsymbol{R}_o$, $\boldsymbol{R}_f$, and $\boldsymbol{R}_z$ represent the recurrent weights of the recurrent data for the input gate, output gate, forget gate, and input unit, respectively. $\boldsymbol{b}_i$, $\boldsymbol{b}_o$, $\boldsymbol{b}_f$, and $\boldsymbol{b}_z$ represent the bias weights for the input gate, output gate, forget gate, and input unit, respectively. $\overline{\boldsymbol{i}^t}$ and $\boldsymbol{i}^t$ represent the input and output data, respectively, of the input gate. $\overline{\boldsymbol{f}^t}$ and $\boldsymbol{f}^t$ represent the input and output data, respectively, of the forget gate. $\overline{\boldsymbol{o}^t}$ and $\boldsymbol{o}^t$ represent the input and output data, respectively, of the output gate. $\overline{\boldsymbol{z}^t}$ and $\boldsymbol{z}^t$ represent the input and output data, respectively, of the input unit. $\boldsymbol{c}^t$ represents the cell stage of the LSTM unit. S represents the sigmoid activation function. T represents the hyperbolic tangent activation function. $\odot$ is the Hadamard product.

4.2 Modelling procedure

The LSTM deep-learning method was first employed for the determination of the axial force and shaft resistance of the cast-in-site piles. The LSTM method was able to extract the nonlinear relationships between the multi-layer soils and the long pile. This is always challenging for the empirical methods owing to the ambiguous knowledge regarding the interaction between the soils and piles. The procedure for building an LSTM model mainly comprises data preparation, architecture determination, and optimisation, as shown in Fig. 11. Each stage is described in detail below.

4.2.1 Dataset preparation

In the data-preparation stage, the input data that contribute to the shaft resistance were judged via the empirical methods. It was concluded that the input data should include the earth pressure coefficient K_0, the vertical effective stress σ'_v, the cohesion c_u, the friction angle φ_u, the undrained shear strength S_u, the thickness of each layer of soil, and the load. The input data for all the soil layers are presented in Table 1. Thus, the input data comprised the soil properties, physical properties, and load. The output data included the axial forces and the shaft resistances of the cast-in-site pile under different loads. Before they were imported into the LSTM model, the input and output data were normalised to the range of 0–1 by dividing by the maximum values. The normalisation

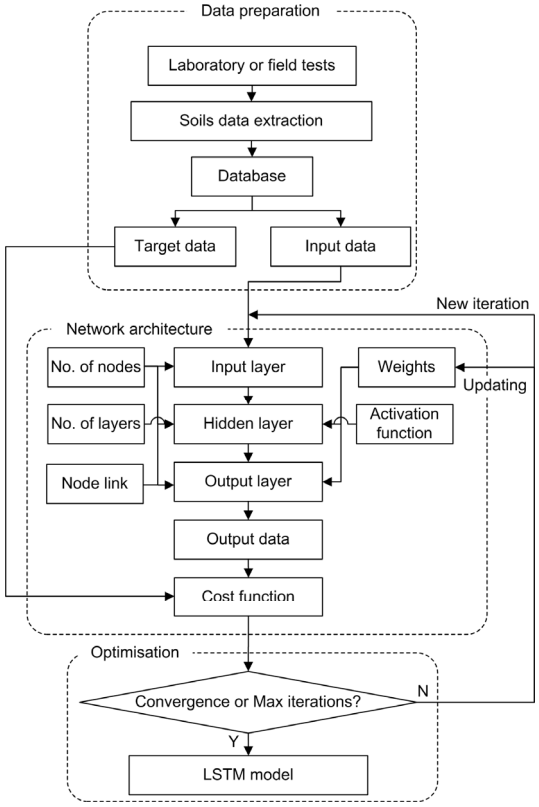

Fig. 11 Modelling procedure of the LSTM method for the shaft resistance evaluation of piles

Table 1 Example of the data input to the LSTM model

Depth (m)	K_0	σ'_v (kPa)	c_u (kPa)	φ_u (°)	S_u (kPa)
0.00	0.58	0.00	9.40	25.00	0.00
4.50	0.58	39.16	9.40	25.00	28.64
10.50	0.89	78.34	9.80	6.60	20.19
17.00	0.89	120.79	9.80	6.60	24.45
20.00	0.73	149.13	35.30	15.40	73.23
23.00	0.78	175.24	25.00	12.50	61.86
29.00	0.72	232.32	41.10	16.20	100.55
36.00	0.76	294.91	36.70	14.10	102.76
38.00	0.78	311.81	29.10	13.00	93.54
43.00	0.70	362.40	44.60	17.30	156.41
49.00	0.77	412.40	31.00	13.20	113.00
58.00	0.77	505.05	31.00	13.20	131.43
68.00	0.71	608.54	43.80	16.60	190.66

played a significant role in training the LSTM model. The dataset comprised seven sets of data measured under the following loads: 2480, 4340, 5580, 6820, 7440, 8680, and 9300 kN. The data measured under the loads of 2480, 4340, 6820, and 8680 kN were used as the training set, and the other data constituted the testing set.

4.2.2 Architectures

Previous studies (Shi et al., 1998; Suwansawat and Einstein, 2006; Santos Jr and Celestino, 2008) indicated that one or two hidden layers in neural networks were sufficient for geotechnical tasks with small datasets, such as ground settlement prediction. Therefore, the LSTM model consisted of two hidden layers, with 12 hidden nodes. The number of nodes in the hidden layers was determined using the trial-and-error method. In this study, the cost function J was the mean squared error function, which is defined as follows:

$$J=\frac{1}{N}\times\sum_{i}^{N}\frac{(y_{\mathrm{p}i}-y_i)^2}{2}+\frac{\lambda}{2N}\times\left(\sum W^1+\sum W^2\right), \quad (8)$$

where N represents the number of training samples, y_i represents the ith set of measured ground settlements, $y_{\mathrm{p}i}$ represents the ith set of predicted ground settlements, and λ is the regularisation parameter which penalizes weights W^1 and W^2 to prevent overfitting (λ=0.1 in this case).

4.2.3 Optimisation

Recently, several stochastic gradient descent algorithms, such as AdaGrad, RMSProp, and Adam, have been developed to train deep-learning networks (Duchi et al., 2011; Kingma and Ba, 2014; Dauphin et al., 2015). These optimisation algorithms allow fast computation for big data tasks at the cost of precision loss at each iteration. Because the database was small in our case, we focused on the stability and accuracy of the optimisation to achieve a higher accuracy. Therefore, the conjugate gradient descent algorithm was used to precisely calculate the gradient descent for each iteration with strict constraints, e.g. the Wolfe–Powell criterion and the linear-search method. The total number of iterations was set at 3000, which is sufficient for small data tasks, according to the authors' experience. Fig. 12 presents the variation of the cost function during the training process. The training process exhibited convergence after nearly 1500 iterations.

4.3 Results and analysis

The training results and predictions of the LSTM model for the axial force and shaft resistance are presented in Figs. 13 and 14, respectively. The LSTM model exhibited an excellent capability for the determination of the axial forces and shaft resistances of the cast-in-site piles on the reclaimed ground. Compared with the results of the empirical methods (Fig. 10), the shaft resistances predicted by the LSTM model agreed closely with the measured data, including the low shaft resistance of the marine mucky clay, the principal resistances of the middle part of the pile, and the decay of the resistance at the end of the pile. Therefore, the LSTM method was suitable for the determination of the axial force and shaft resistance of the cast-in-site piles, outperforming the empirical methods with regard to precision.

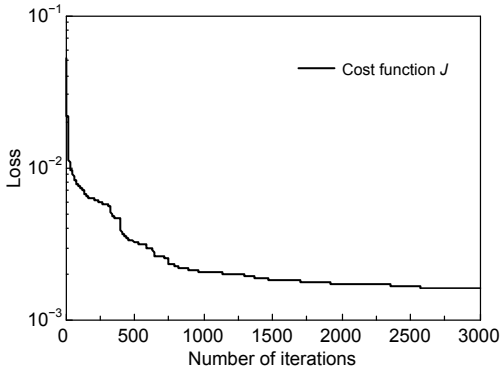

Fig. 12 Loss development during the training process

The performance of the LSTM model was evaluated according to the root mean square error (RMSE) and coefficient of determination (R^2). RMSE and R^2 are given by

$$\mathrm{RMSE}=\sqrt{\frac{1}{N}\sum_{j}^{N}(y_{\mathrm{p}j}-y_j)^2}, \quad (9)$$

$$R^2=1-\frac{\sum_{j}^{N}(y_j-y_{\mathrm{p}j})^2}{\sum_{j}^{N}(y_j-\bar{y})^2}, \quad (10)$$

where j indicates the set of input data, N represents the number of training or testing samples, and $\bar{y}$ represents the mean value of the measured ground settlements.

The coefficients of determination (R^2) and RMSE are presented in Table 2. A larger coefficient of determination and smaller RMSE indicate better prediction performance. The R^2 values for the axial

force of the LSTM model were >0.99 for both the training and testing sets. The R^2 values for the shaft resistance were >0.92 under different loads. The maximum value of RMSE of the predicted axial force was only 150 kN, which was <3% of the ultimate load (9300 kN). The maximum value of RMSE of the shaft resistance was <12 kPa, which was far smaller than that of the empirical method. The large coefficients of determination and small RMSEs indicate the excellent capability of the LSTM model on learning and reasoning the axial force and shaft resistance of the cast-in-site piles on the reclaimed ground.

Table 2 Evaluation indices for the performance of the LSTM model

Dataset	Load (kN)	R^2		RMSE	
		Axial force	Shaft resistance	Axial force (kN)	Shaft resistance (kPa)
Training	2480	0.993	0.977	95.28	2.13
	4340	0.996	0.983	80.78	4.36
	6820	0.998	0.986	91.64	11.60
	8680	0.998	0.944	105.48	4.81
Testing	5580	0.999	0.921	159.18	11.60
	7440	0.996	0.986	124.4	4.81
	9300	0.995	0.944	150.44	10.12

Despite the aforementioned advantages of this intelligent method, at present, the trained LSTM model is only appropriate for a positive shaft resistance under static loading. A negative shaft resistance can be significant for a pile embedded in soft soils, particularly in under-consolidated soils. In this study, the field loading test was conducted over 2 d, whereas the consolidation of the surrounding ground requires a far longer time. The objective of the study was to validate a new intelligent approach for determining the variation of the shaft resistance under the loading process using field test data. In the field tests, the settlements of the piles were significantly higher than the soils around the piles, and a negative skin friction was not observed. Therefore, in this study,

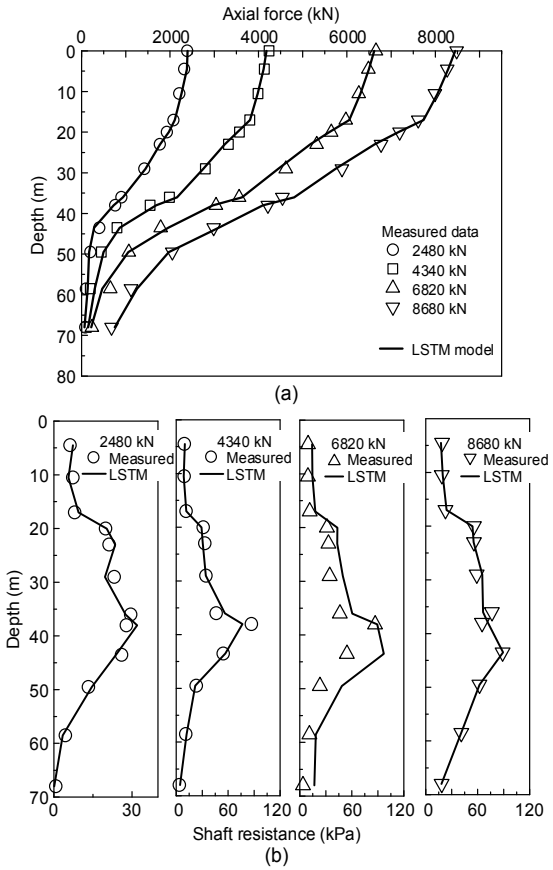

Fig. 13 Training performance of the LSTM model under different loads for pile P16: (a) axial force; (b) shaft resistance

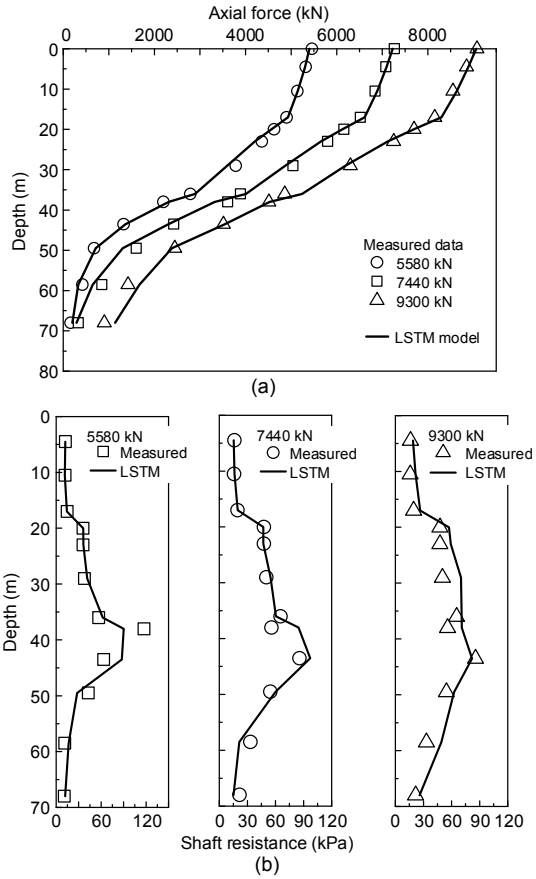

Fig. 14 Predictions of the LSTM model under different loads for pile P16: (a) axial force; (b) shaft resistance

the shaft resistances of the soils were generally positive skin resistances. The intelligent model was trained using the measured axial force and shaft resistance, which represent the interactions between the piles and soils. In the future, when the long-term operation load is considered, the negative skin resistance may be significant. This can be considered by an intelligent model similar to the proposed LSTM model. The development of an LSTM model for the negative skin resistance is recommended for a future study.

5 Conclusions

By performing field tests and using an LSTM deep-learning method, we investigated the axial forces and shaft resistances of cast-in-site piles on reclaimed ground. According to the results, the following conclusions are drawn.

1. A series of field tests was performed to investigate the working states of the cast-in-site piles on the reclaimed ground. The cast-in-site piles bear the designed load on the reclaimed ground mainly through their shaft resistances. Most of the shaft resistances come from the middle of the piles. The thick marine mucky clay can only bear 10% of the load, owing to its poor mechanical properties.

2. The ultimate shaft resistance of the cast-in-site pile was assessed via empirical methods. Generally, the empirical methods accurately estimated the ultimate shaft resistance of the middle of the pile. Larger biases of the estimated shaft resistance occurred at the top and end of the pile, indicating the limitation of the empirical methods for the reclaimed ground.

3. The proposed intelligent approach based on the LSTM deep-learning technique predicted the axial force and shaft resistance with high accuracy not only in the ultimate bearing state of the pile but also in the normal working state. By learning the data for the normal working state, the LSTM model successfully predicted the ultimate shaft resistance under the ultimate bearing load.

Contributors

Sheng-liang LU designed the research and conducted the field test. Ning ZHANG conducted the LSTM analysis and drafted the manuscript. Hu-zhong LI conducted the data processing. Shui-long SHEN and Annan ZHOU supervised the project, proposed the scheme of the field test, and revised the final version.

Conflict of interest

Sheng-liang LU, Ning ZHANG, Shui-long SHEN, Annan ZHOU, and Hu-zhong LI declare that they have no conflict of interest.

References

Abu Kiefa MA, 1998. General regression neural networks for driven piles in cohesionless soils. *Journal of Geotechnical and Geoenvironmental Engineering*, 124(12):1177-1185. https://doi.org/10.1061/(asce)1090-0241(1998)124:12(1177)

Alkroosh I, Nikraz H, 2012. Predicting axial capacity of driven piles in cohesive soils using intelligent computing. *Engineering Applications of Artificial Intelligence*, 25(3):618-627. https://doi.org/10.1016/j.engappai.2011.08.009

Ardalan H, Eslami A, Nariman-Zadeh N, 2009. Piles shaft capacity from CPT and CPTu data by polynomial neural networks and genetic algorithms. *Computers and Geotechnics*, 36(4):616-625. https://doi.org/10.1016/j.compgeo.2008.09.003

Atangana Njock PG, Shen SL, Zhou AN, et al., 2020. Evaluation of soil liquefaction using AI technology incorporating a coupled ENN/t-SNE model. *Soil Dynamics and Earthquake Engineering*, 130:105988. https://doi.org/10.1016/j.soildyn.2019.105988

Baziar MH, Kashkooli A, Saeedi-Azizkandi A, 2012. Prediction of pile shaft resistance using Cone Penetration Tests (CPTs). *Computers and Geotechnics*, 45:74-82. https://doi.org/10.1016/j.compgeo.2012.04.005

Behrmann JH, Meissl S, 2012. Submarine landslides, Gulf of Mexico continental slope: insights into transport processes from fabrics and geotechnical data. *In*: Yamada Y, Kawamura K, Ikehara K, et al. (Eds.), Submarine Mass Movements and Their Consequences. Springer, Dordrecht, the Netherland, p.463-472. https://doi.org/10.1007/978-94-007-2162-3_41

Bustamante M, Gianeselli L, 1982. Pile bearing capacity prediction by means of static penetrometer CPT. Proceedings of the 2nd European Symposium Penetration Testing, p.493-500.

Cai YQ, Xie ZW, Wang J, et al., 2018. New approach of vacuum preloading with booster prefabricated vertical drains (PVDs) to improve deep marine clay strata. *Canadian Geotechnical Journal*, 55(10):1359-1371. https://doi.org/10.1139/cgj-2017-0412

Chai JC, Shen JSL, Liu MD, et al., 2018. Predicting the performance of embankments on PVD-improved subsoils. *Computers and Geotechnics*, 93:222-231. https://doi.org/10.1016/j.compgeo.2017.05.018

Chan WT, Chow YK, Liu LF, 1995. Neural network: an alternative to pile driving formulas. *Computers and Geotechnics*, 17(2):135-156.

https://doi.org/10.1016/0266-352X(95)93866-H

Dauphin YN, de Vries H, Bengio Y, 2015. Equilibrated adaptive learning rates for non-convex optimization. *Advances in Neural Information Processing Systems*, 35(3):1504-1512.

de Kuiter J, Beringen FL, 1979. Pile foundations for large North Sea structures. *Marine Geotechnology*, 3(3):267-314.
https://doi.org/10.1080/10641197909379805

Duchi J, Hazan E, Singer Y, 2011. Adaptive subgradient methods for online learning and stochastic optimization. *The Journal of Machine Learning Research*, 12:257-269.

Elbaz K, Shen SL, Sun WJ, et al., 2020. Prediction model of shield performance during tunneling via incorporating improved particle swarm optimization into ANFIS. *IEEE Access*, 8(1):39659-39671.
https://doi.org/10.1109/ACCESS.2020.2974058

Fang K, Pan M, Shen CP, 2019. The value of SMAP for long-term soil moisture estimation with the help of deep learning. *IEEE Transactions on Geoscience and Remote Sensing*, 57(4):2221-2233.
https://doi.org/10.1109/TGRS.2018.2872131

Formela K, Wąsowicz D, Formela M, et al., 2015. Curing characteristics, mechanical and thermal properties of reclaimed ground tire rubber cured with various vulcanizing systems. *Iranian Polymer Journal*, 24(4):289-297.
https://doi.org/10.1007/s13726-015-0320-9

Gers FA, Schraudolph NN, Schmidhuber J, 2003. Learning precise timing with LSTM recurrent networks. *The Journal of Machine Learning Research*, 3:115-143.
https://doi.org/10.1162/153244303768966139

Ghorbani B, Sadrossadat E, Bazaz JB, et al., 2018. Numerical ANFIS-based formulation for prediction of the ultimate axial load bearing capacity of piles through CPT data. *Geotechnical and Geological Engineering*, 36(4):2057-2076.
https://doi.org/10.1007/s10706-018-0445-7

Goh ATC, 1996. Pile driving records reanalyzed using neural networks. *Journal of Geotechnical Engineering*, 122(6):492-495.
https://doi.org/10.1061/(asce)0733-9410(1996)122:6(492)

Goh ATC, Kulhawy FH, Chua CG, 2005. Bayesian neural network analysis of undrained side resistance of drilled shafts. *Journal of Geotechnical and Geoenvironmental Engineering*, 131(1):84-93.
https://doi.org/10.1061/(asce)1090-0241(2005)131:1(84)

Ji F, Ding JW, Hong ZS, et al., 2011. Experimental study on dewatering dredged clay with ventilating vacuum method. *Advanced Materials Research*, 261-263:1650-1654.
https://doi.org/10.4028/www.scientific.net/AMR.261-263.1650

Jin YF, Yin ZY, Wu ZX, et al., 2018a. Identifying parameters of easily crushable sand and application to offshore pile driving. *Ocean Engineering*, 154:416-429.
https://doi.org/10.1016/j.oceaneng.2018.01.023

Jin YF, Yin ZY, Wu ZX, et al., 2018b. Numerical modeling of pile penetration in silica sands considering the effect of grain breakage. *Finite Elements in Analysis and Design*, 144:15-29.
https://doi.org/10.1016/j.finel.2018.02.003

Karlsrud K, Clausen CJF, Aas PM, 2005. Bearing capacity of driven piles in clay, the NGI approach. Proceedings of International Symposium on Frontiers in Offshore Geotechnics, p.775-782.

Kingma DP, Ba J, 2014. Adam: a method for stochastic optimization. arXiv:1412.6980.

Kong LG, Fan JY, Liu JW, et al., 2019. Group effect in piles under eccentric lateral loading in sand. *Journal of Zhejiang University-SCIENCE A (Applied Physics & Engineering)*, 20(4):243-257.
https://doi.org/10.1631/jzus.A1800617

Lee IM, Lee JH, 1996. Prediction of pile bearing capacity using artificial neural networks. *Computers and Geotechnics*, 18(3):189-200.
https://doi.org/10.1016/0266-352X(95)00027-8

Li AG, Tham LG, Wen JP, et al., 2014. Case study of ground improvement to Qianhai reclamation area, Qianhai Bay, Shenzhen. Proceedings of Geo-Shanghai, p.231-240.
https://doi.org/10.1061/9780784413401.023

Li S, Yue ZQ, Tham LG, et al., 2005. Slope failure in underconsolidated soft soils during the development of a port in Tianjin, China. Part 2: analytical study. *Canadian Geotechnical Journal*, 42(1):166-183.
https://doi.org/10.1139/t04-088

Ling Z, Wang WD, Wu JB, et al., 2018. Shaft resistance of pre-bored precast piles in Shanghai clay. *Proceedings of the Institution of Civil Engineers-Geotechnical Engineering*, 172(3):228-242.
https://doi.org/10.1680/jgeen.18.00028

Liu YX, Jiang SP, Zhao YM, 2004. Testing study on mechanical characteristics of natural underconsolidated soils. *Chinese Journal of Rock Mechanics and Engineering*, 23(S1):4409-4413 (in Chinese).
https://doi.org/10.3321/j.issn:1000-6915.2004.z1.029

Lyu HM, Shen SL, Zhou AN, et al., 2019a. Flood risk assessment of metro systems in a subsiding environment using the interval FAHP-FCA approach. *Sustainable Cities and Society*, 50:101682.
https://doi.org/10.1016/j.scs.2019.101682

Lyu HM, Shen SL, Yang J, et al., 2019b. Inundation analysis of metro systems with the storm water management model incorporated into a geographical information system: a case study in Shanghai. *Hydrology and Earth System Sciences*, 23(10):4293-4307.
https://doi.org/10.5194/hess-23-4293-2019

Lyu HM, Shen SL, Yang J, et al., 2020a. Risk assessment of earthquake-triggered geohazards surrounding Wenchuan, China. *Natural Hazards Review*, 21(3):05020003.
https://doi.org/10.1061/(ASCE)NH.1527-6996.0000375

Lyu HM, Shen SL, Zhou AN, et al., 2020b. Risk assessment of mega-city infrastructures related to land subsidence using improved trapezoidal FAHP. *Science of the Total*

Environment, 717:135310.
https://doi.org/10.1016/j.scitotenv.2019.135310

Lyu HM, Sun WJ, Shen SL, et al., 2020c. Risk assessment using a new consulting process in fuzzy AHP. *Journal of Construction Engineering and Management*, 146(3): 04019112.
https://doi.org/10.1061/(ASCE)CO.1943-7862.0001757

Ma HP, Chen ZY, Yu S, 2014. Correlations of soil shear strength with specific penetration resistance of CPT in shanghai area. *Rock and Soil Mechanics*, 35(2):536-542 (in Chinese).
https://doi.org/10.16285/j.rsm.2014.02.021

Mayne PW, Kulhawy FH, 1982. K_0-OCR relationships in soil. *Journal of the Geotechnical Engineering Division*, 108(6):851-872.

MOHURD (Ministry of Housing and Urban-Rural Development of the People's Republic of China), 2014. Technical Code for Testing of Building Foundation Piles, JGJ106-2014. National Standards of the People's Republic of China (in Chinese).

Nonaka T, Yamada S, Noda T, 2017. Soil-water coupled analysis of pore water pressure dissipation in performance design-examinations of effectiveness in reclaimed ground. *Geotechnical Engineering*, 48(4):19-31.

O'Neill MW, Reese LC, 1999. Drilled Shafts: Construction Procedures and Design Methods. No. FHWA-IF-99-025, US Department of Transportation, Federal Highway Administration, Washington DC, USA.

Park HI, Cho CW, 2010. Neural network model for predicting the resistance of driven piles. *Marine Georesources & Geotechnology*, 28(4):324-344.
https://doi.org/10.1080/1064119X.2010.514232

Randolph MF, Murphy BS, 1985. Shaft capacity of driven piles in clay. Proceedings of the 17th Annual Offshore Technology Conference, p.371-378.

Sak H, Senior AW, Beaufays F, 2014. Long short-term memory recurrent neural network architectures for large scale acoustic modeling. Proceedings of the Fifteenth Annual Conference of the International Speech Communication Association, p.338-342.

Santos Jr OJ, Celestino TB, 2008. Artificial neural networks analysis of São Paulo subway tunnel settlement data. *Tunnelling and Underground Space Technology*, 23(5): 481-491.
https://doi.org/10.1016/j.tust.2007.07.002

Sarir P, Shen SL, Wang ZF, et al., 2019. Optimum model for bearing capacity of concrete-steel columns with AI technology via incorporating the algorithms of IWO and ABC. *Engineering with Computers*, in press.
https://doi.org/10.1007/s00366-019-00855-5

Shahin MA, 2010. Intelligent computing for modeling axial capacity of pile foundations. *Canadian Geotechnical Journal*, 47(2):230-243.
https://doi.org/10.1139/T09-094

Shen MF, Martin JR, Ku CS, et al., 2018. A case study of the effect of dynamic compaction on liquefaction of reclaimed ground. *Engineering Geology*, 240:48-61.
https://doi.org/10.1016/j.enggeo.2018.04.003

Shen SL, Chai JC, Hong ZS, et al., 2005. Analysis of field performance of embankments on soft clay deposit with and without PVD-improvement. *Geotextiles and Geomembranes*, 23(6):463-485.
https://doi.org/10.1016/j.geotexmem.2005.05.002

Shen SL, Wu YX, Misra A, 2017. Calculation of head difference at two sides of a cut-off barrier during excavation dewatering. *Computers and Geotechnics*, 91:192-202.
https://doi.org/10.1016/j.compgeo.2017.07.014

Shi JS, Ortigao JAR, Bai JL, 1998. Modular neural networks for predicting settlements during tunneling. *Journal of Geotechnical and Geoenvironmental Engineering*, 124(5):389-395.
https://doi.org/10.1061/(asce)1090-0241(1998)124:5(389)

Suwansawat S, Einstein HH, 2006. Artificial neural networks for predicting the maximum surface settlement caused by EPB shield tunneling. *Tunnelling and Underground Space Technology*, 21(2):133-150.
https://doi.org/10.1016/j.tust.2005.06.007

Teh CI, Wong KS, Goh ATC, et al., 1997. Prediction of pile capacity using neural networks. *Journal of Computing in Civil Engineering*, 11(2):129-138.
https://doi.org/10.1061/(asce)0887-3801(1997)11:2(129)

Wang K, Sun WC, 2018. A multiscale multi-permeability poroplasticity model linked by recursive homogenizations and deep learning. *Computer Methods in Applied Mechanics and Engineering*, 334:337-380.
https://doi.org/10.1016/j.cma.2018.01.036

Wang XW, Yang TL, Xu YS, et al., 2019. Evaluation of optimized depth of waterproof curtain to mitigate negative impacts during dewatering. *Journal of Hydrology*, 577: 123969.
https://doi.org/10.1016/j.jhydrol.2019.123969

Wang ZF, Shen JS, Cheng WC, 2018. Simple method to predict ground displacements caused by installing horizontal jet-grouting columns. *Mathematical Problems in Engineering*, 2018:1897394.
https://doi.org/10.1155/2018/1897394

Wang ZF, Shen SL, Modoni G, 2019. Enhancing discharge of spoil to mitigate disturbance induced by horizontal jet grouting in clayey soil: theoretical model and application. *Computers and Geotechnics*, 111:222-228.
https://doi.org/10.1016/j.compgeo.2019.03.012

Wu YX, Shen SL, Lyu HM, et al., 2020. Analyses of leakage effect of waterproof curtain during excavation dewatering. *Journal of Hydrology*, 583:124582.
https://doi.org/10.1016/j.jhydrol.2020.124582

Xu YS, Yan XX, Shen SL, et al., 2019. Experimental investigation on the blocking of groundwater seepage from a waterproof curtain during pumped dewatering in an excavation. *Hydrogeology Journal*, 27(7):2659-2672.
https://doi.org/10.1007/s10040-019-01992-3

Yan SW, Chu J, 2005. Soil improvement for a storage yard using the combined vacuum and fill preloading method.

Canadian Geotechnical Journal, 42(4):1094-1104. https://doi.org/10.1139/t05-042

Yao YP, Yamamoto H, Wang ND, 2008a. Constitutive model considering sand crushing. *Soils and Foundations*, 48(4): 603-608. https://doi.org/10.3208/sandf.48.603

Yao YP, Sun DA, Matsuoka H, 2008b. A unified constitutive model for both clay and sand with hardening parameter independent on stress path. *Computers and Geotechnics*, 35(2):210-222. https://doi.org/10.1016/j.compgeo.2007.04.003

Yin ZY, Jin YF, Shen SL, et al., 2017. An efficient optimization method for identifying parameters of soft structured clay by an enhanced genetic algorithm and elastic-viscoplastic model. *Acta Geotechnica*, 12(4):849-867. https://doi.org/10.1007/s11440-016-0486-0

Yin ZY, Wu ZY, Hicher PY, 2018a. Modeling monotonic and cyclic behavior of granular materials by exponential constitutive function. *Journal of Engineering Mechanics*, 144(4):04018014. https://doi.org/10.1061/(ASCE)EM.1943-7889.0001437

Yin ZY, Jin YF, Shen SL, et al., 2018b. Optimization techniques for identifying soil parameters in geotechnical engineering: comparative study and enhancement. *International Journal for Numerical and Analytical Methods in Geomechanics*, 42(1):70-94. https://doi.org/10.1002/nag.2714

Zhang N, Shen SL, Wu HN, et al., 2015. Evaluation of effect of basal geotextile reinforcement under embankment loading on soft marine deposits. *Geotextiles and Geomembranes*, 43(6):506-514. https://doi.org/10.1016/j.geotexmem.2015.05.005

Zhang N, Shen SL, Zhou AN, et al., 2019. Investigation on performance of neural networks using quadratic relative error cost function. *IEEE Access*, 7:106642-106652. https://doi.org/10.1109/ACCESS.2019.2930520

Zhou AN, Huang RQ, Sheng DC, 2016. Capillary water retention curve and shear strength of unsaturated soils. *Canadian Geotechnical Journal*, 53(6):974-987. https://doi.org/10.1139/cgj-2015-0322

Zhou AN, Wu SS, Li J, et al., 2018. Including degree of capillary saturation into constitutive modelling of unsaturated soils. *Computers and Geotechnics*, 95:82-98. https://doi.org/10.1016/j.compgeo.2017.09.017

Zhou JJ, Wang KH, Gong XN, et al., 2013. Bearing capacity and load transfer mechanism of a static drill rooted nodular pile in soft soil areas. *Journal of Zhejiang University-SCIENCE A (Applied Physics & Engineering)*, 14(10): 705-719. https://doi.org/10.1631/jzus.A1300139

Zhou M, Liu HL, Hossain MS, et al., 2016. Numerical simulation of plug formation during casing installation of cast-in-place concrete pipe (PCC) piles. *Canadian Geotechnical Journal*, 53(7):1093-1109. https://doi.org/10.1139/cgj-2015-0162

Zhou XH, Shen SL, Xu YS, et al., 2019. Analysis of production safety in the construction industry of China in 2018. *Sustainability*, 11(17):4537. https://doi.org/10.3390/su11174537

中文概要

题　目：基于现场试验的复垦地层灌注桩侧摩阻力的深度学习评价方法

目　的：基于极限平衡理论和诸多简化原则的经验公式方法难以适用于复杂的复垦地层中灌注桩的侧摩阻力计算。本文旨在探讨复垦地层中灌注桩在静力加载条件下的侧摩阻力发展规律和特性，并应用深度学习方法，以提高灌注桩侧摩阻力的预测精度。

创新点：1. 设计现场试验，研究近海复垦地层中灌注桩的承载能力特性；2. 建立深度学习预测模型，高精度预测工作荷载下灌注桩的轴力和侧摩阻力。

方　法：1. 通过实验分析，探明复垦地层中不同土层与桩体的相互作用和桩体侧摩阻力的发展规律；2. 通过理论计算，指出经验方法在复垦地层灌注桩承载力计算中的缺陷和不足；3. 通过序列化的人工智能方法建模，利用土体物理力学参数和桩身试验实测数据，对比验证深度学习方法的精度和计算效率。

结　论：1. 灌注桩适用于复垦地层，能够为基础设施提供足够的承载力；2. 经验方法对灌注桩中部桩体的极限侧摩阻力估计良好，而对地层条件较差的桩身两端的估计则存在较大偏差；3. 深度学习方法能够综合考虑地层和桩体的相互作用，并且能精确预测在不同工作荷载和极限荷载下的侧摩阻力和桩身轴力，因而适用性更广。

关键词：深度学习方法；灌注桩；侧摩阻力；现场试验；复垦地层